COBEM 2021 26th International Congress of Mechanical Engineering
November 22-26, 2021, Virtual Congress, Brazil
ABCM Associação Brasileira de Engenharia e Ciências Mecânicas

COB-2021-1978
RECEPTIVITY OF ACOUSTIC WAVES ON LOCALIZED ROUGHNESS IN COMPRESSIBLE LAMINAR BOUNDARY LAYERS

Pedro Henrique Rosa dos Santos
São Carlos School of Engineering, University of São Paulo, USP
pedrorosasantos@usp.br

Fernando H. T. Himeno
fernando.himeno@usp.br

Marlon Sproesser Mathias
marlon.mathias@usp.br

Marcello Augusto Faraco de Medeiros
marcello@sc.usp.br

Abstract. *Surface imperfections, such as roughnesses, can affect the laminar-turbulent transition process in boundary layers. One main engineering objective is predicting the initial amplitude of instability waves, which is a function of the flow's receptivity to external disturbances. Existing theories about receptivity are limited to restricted flow regimes and semi-empirical relations are commonly used in industry. In this context, this paper investigates the receptivity of the scattering of one-dimensional acoustic waves on roughness located in a flat plate boundary layer. To do so, this work carried out high-order DNS simulations of a roughness inserted in a flat plate boundary layer. A sinusoidal velocity perturbation with constant frequency was superimposed on the inflow contour of the base flow. The Tollmien Schilichting wave is obtained by the difference between the unsteady fluctuation of the cases with and without roughness. The data is compared with recent experiments and the numerical uncertainty is quantified.*

Keywords: *Receptivity, Laminar-Turbulent Transition, DNS, Tollmien-Schlichting waves*

1. INTRODUCTION

Turbulence in boundary layers plays a critical role in the net drag force on vehicles, which in turn has a significant impact on fuel consumption and pollutant emissions. Since the environmental footprint and the operational cost are some of the major concerns nowadays, the aeronautical industry has been seeking new technologies to optimize the turbulence effects, such as the hybrid laminar flow design. Some estimates say that it is possible to achieve a 5% reduction in fuel consumption by extending the laminar boundary layer (Raposo *et al.*, 2019). Although the mechanisms that underpin the turbulence are not fully understood, one may rely on the process which leads to the transition from laminar to turbulent flow to optimize a vehicle design for enhanced energetic efficiency. In the design phase, one of the main objectives is to precisely predict the position of the laminar-turbulent transition, which is sensitive to external disturbances (such as acoustic, vortical, and entropy disturbance) and surface irregularities (such as humps and gaps). This prediction demands a clear understanding of the transitional process that accounts for external perturbations and surface irregularities.

Several studies over the last century have established that wave instabilities within the boundary layer are pivotal to the laminar-turbulent transition process. Moreover, the previous studies commonly acknowledge that this process has three stages: receptivity, instability growth, and breakdown. The term "receptivity" traces back to Morkovin (1969), and it stands for the introduction of wave instabilities into the boundary layer. Besides, "natural receptivity" can be defined, according to Saric *et al.* (2002), as the mechanism responsible for the transference of energy from the external free-stream disturbances to the instability waves in the boundary layer, such as the Tollmien-Schilichting waves in the subsonic flow. What is more, Ruban (1984) argues that the receptivity is prone to occur in regions of rapid change in mean flow, such as in the leading edge or the near field of surface non uniformities. The reason is the necessity of a scale conversion mechanism, as the external disturbances usually have a different wavelength from the instabilities modes' wavelength. Thus, this mechanism determines the initial amplitude, phase, and frequency of the instability waves. In low disturbances environments, such as the atmospheric flight of an airliner, the instabilities waves introduced via receptivity amplify most through linear modes. However, in higher disturbances scenarios with lesser surface finish, it is possible to occur bypass transition (Morkovin, 1994). Ultimately, these waves amplify, and nonlinear effects arise, giving birth to the breakdown

of turbulence.

Calculation of receptivity can be found on Ruban (1984), which utilizes asymptotic expansion, and on Crouch (1992), which utilizes a finite Reynolds number theory. Both of them utilize an incompressible set of governing equations, and they are best suited for first branch receptivity, not second branch. With few exceptions, previous works in the literature often relied on this incompressible approximation.

More recent studies started investigating the influence of compressibility on the stability and receptivity, among other parameters. The work of De Tullio and Ruban (2015) presents a Direct Numerical Simulation (DNS) of the receptivity of several flow conditions to acoustic incidence on a localized bump of a gaussian shape, whose height, h, is less than 0,01% of the displacement thickness of the undisturbed boundary layer at the roughness position, δ_b^*. They compared the results from the asymptotic prediction, and they found agreement of the order of 10%. They also extended the analysis to different roughness height and found that at about $h = 0.17\delta_b^*$ the receptivity becomes nonlinear, which is in agreement with Crouch (1992), and this height is independent of Reynolds number. However, the scheme utilized has a linearization technique, and may not be fully extensible to the nonlinear regime.

The study of Raposo *et al.* (2019) made use of Adjoint Harmonic Linearised Navier Stokes Equations (AHLNS) to solve the localized roughness acoustic receptivity problem, and also utilized asymptotic expansion theory, as well as the work of De Tullio and Ruban (2015), as a benchmark. Their methodology showed remarkable accuracy and computational efficiency, yet it does not handle other flow configurations. They reported a strong dependence on Mach number, roughness streamwise position and acoustic non dimensional frequency, $F = (2\pi f_{exc}\nu)/U_\infty^2$, on the receptivity. In this equation, f_{exc} is the dimensional frequency in Hertz, ν is the kinematic viscosity and U_∞ is the free stream velocity. The difference of the receptivity between a localized roughness at the first branch in a flow with Mach number 0.1 and 0.5, both with $F = 20 \times 10^{-6}$, changed by a factor of 2.2, approximately.

Placidi *et al.* (2020) utilized a technique based on a vanishing 2D roughness to bypass some of these limitations. Their results showed a departure from the linear regime at about $h > 0.126\delta_b^*$. They compared their results with the data from the code described by Raposo *et al.* (2019), and the results agreed very well in the linear receptivity regime. However, the mentioned code has not the ability to provide data for the receptivity in the non-linear regime.

On the one hand, experimental works utilized a variety of approaches to measure the instability wave due to acoustic scattering on roughness with several heights, and each these approaches has limitations either on the robustness, accuracy, or acquisition procedure. On the other hand, numerical studies provided some relevant results with a recent progress in compressible subsonic regime. However, they are constrained to the linear regime of receptivity. The roughness' height in these numerical studies are often limited to the first scale of the triple-deck assympotic theory from Ruban (1984).

As discussed above, there is a recent research effort on the compressibility effects in the receptivity and on its non-linear behavior. The DNS simulation has the potential to provide data about the receptivity of higher roughness' height, outside the first triple-deck scaling. In this context, the general objective of this paper is to perform numerical simulations of the scattering of acoustic waves over localized roughness on boundary layers in order to assess the non linear receptivity regime in the future. The first specific objective is to quantify the uncertainty associated with the numerical procedure. The second specific objective is to compare the experimental results from Placidi *et al.* (2020) yet in the linear receptivity regime. The third specific objective, which is yet to be done, is to assess the departure from linear regime of receptivity and compare the full parametric space from Placidi *et al.* (2020).

The remaining of this paper is organized as follows. The second section describes the simulation's parameters. The third section describes briefly the numerical procedure of the Direct Navier Stokes code developed in-house. The fourth section presents some results concerning to the uncertainty study. The fifth section provides visualization of the flow. The sixth section is dedicated to the comparison with the available experimental data. Then, the conclusion and next steps are delineated in the seventh section.

2. PROBLEM FORMULATION

The present work carried out DNS simulations with a high order finite difference scheme. The geometries were flat plates with and without roughness. The computational model used is shown in Fig 1. In this figure, L is the distance from leading edge to the upstream edge of the roughness. h and w are the height and the width of the hump, respectively.

The boundary conditions are also described in Fig. 1. The acoustic inlet is a region designed to minimize the error associated with the miscalculation of the acoustic impedance at the inflow. The buffer zone region is designed to dissipate both the acoustic and Tollmien-Schilichting waves, and there is a numerical damping in this region. This numerical damping is explained in section 3.

The relevant flow parameters are summarized in Tab. 1. It reports the following non-dimensional numbers: $Re_\infty = U_\infty h/\nu$, $Re_{hh} = U(h)h/\nu$, and $Re_{\delta_b^*} = U_\infty \delta_b^*/\nu$. These numbers are the Reynolds number based on the free stream velocity, the Reynolds number based on roughness height and the velocity at roughness height ($U(h)$), and the Reynolds number based on the displacement thickness of the undisturbed blasius' profile, δ_b^*, respectively. These parameters are calculated at the position of the upstream edge of the hump. The useful domain range is [-100 1200]x[0 38], in terms of δ_b^*.

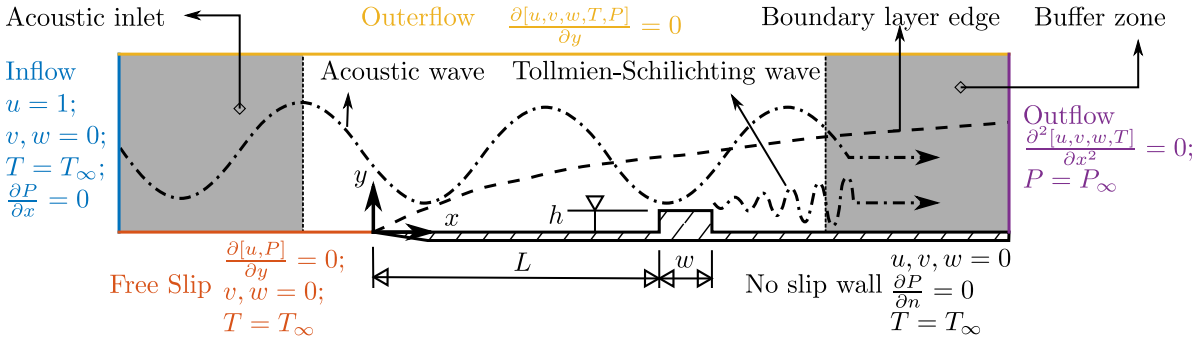

Figure 1. Geometry and boundary conditions of the computational model.

Table 1. Flow parameters.

Re_∞	Re_{hh}	$Re_{\delta_b^*}$	Ma	$F \times 10^6$	h/δ_b^*	w/h
178.09	12.71	1415.58	0.10	25.00	12.58%	133.33

The Fig. 2 presents the stability diagram obtained by the solution of the Orr-Sommerfeld equation. In this figure, the blue dot is drawn at the parametric space in Tab. 1. It is possible to see that the roughness is near to the first branch of the Tollmien-Schilichting wave.

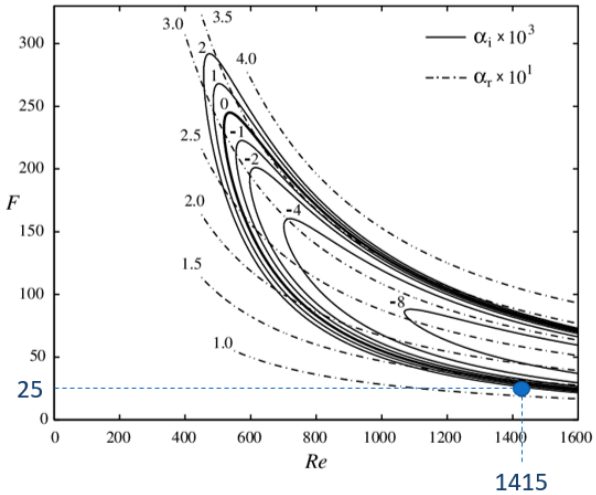

Figure 2. Stability chart of the Tollmien-Schilichting wave over the smooth plate. The solid (–) lines are the imaginary wave numbers (α_i) contour levels. The dashed lines (- -) are the real wave numbers (α_r) contour levels. The weighted solid line is the neutral curve. The blue dot is the representation of the parametric space in study. The characteristic length is the local displacement thickness, δ^*.
Adapted from Fransson (2003)

The baseflows obtained were superimposed by a sinusoidal wave at the inflow boundary condition. It had a constant non-dimensional frequency matching the experimental frequency from Placidi *et al.* (2020) and it has an amplitude of $\mathcal{O}(U_\infty \times 10^{-3})$, where U_∞ is the reference far-field velocity. This amplitude is thought to be inside of the linear regime, as it will be addressed in the next sections. It is consistent with 100 dB in the flat plate of Placidi *et al.* (2020). The Tollmien Schilichting waves generated via receptivity were filtered out using the subtraction between the fluctuations from the cases with and without roughness. This is showed in section 5.

3. NUMERICAL SCHEME

Equations 1 to 3 presents the Compressible Navier-Stokes Equations that are directly solved via finite difference method with explicit fourth-order Runge-Kutta time marching scheme. The primitive variables are evaluated at each node in dimensionless form. In these equations, which are in index notation, ρ is specific mass, t is time, u_i is the velocity at

the x_i direction, p is pressure, τ_{ij} is shear stress, e is internal energy, q_i is heat flux in the x_i direction.

$$\frac{\partial \rho}{\partial t} = -\rho \frac{\partial u_i}{\partial x_i} - \frac{\partial \rho}{\partial x_i} u_i \tag{1}$$

$$\frac{\partial u_j}{\partial t} = -\frac{\partial u_j}{\partial x_i} u_i - \frac{1}{\rho} \frac{\partial p}{\partial x_j} + \frac{1}{\rho} \frac{\partial \tau_{ij}}{\partial x_i} \tag{2}$$

$$\frac{\partial e}{\partial t} = -\frac{\partial e}{\partial x_i} u_i - \frac{p}{\rho} \frac{\partial u_i}{\partial x_i} - \frac{1}{\rho} \frac{\partial q_i}{\partial x_i} \tag{3}$$

The code uses structured mesh in a rectangular domain. There is stretching in both X and Y directions. It is possible to control the strength and size of the stretching. Care is taken to slightly modify the node position to match the roughness edges. The grid is much finer close to the wall and roughness. The mesh is shown in Fig. 3.

Both the flat plate and the roughness walls have no-slip and no-penetration boundary conditions, as well as zero pressure gradient in the normal direction and constant temperature. The pressure in both roughness' corners nodes is set to the mean of the pressures that meet the boundary condition for each direction. Upstream of the flat plate there is a free-slip region to represent free flow before the leading edge of the no-slip wall. This free-slip region allows the pressure gradients just before the boundary layer to be computed.

Following the Fig. 1, the upper boundary has a null Neumann boundary condition. In the outflow, the second derivatives are set to zero, except for the pressure. The pressure is defined with Dirichlet boundary condition in outflow boundary condition and null Neumann in the inflow boundary condition. For the acoustic wave, a harmonic perturbation is superimposed at the inflow. Due to the acoustic impedance miscalculation, a carefully stretched region is placed at the inlet to dissipate spurious oscillations. A buffer zone downstream exists so oscillations are neither reflected nor amplified. It is a non-physical region where the node spacing is increased, the spatial derivative has a decreased order and there is a selective frequency damping low-pass filter (Åkervik *et al.*, 2006).

The finite difference scheme has sixth-order spectral-like accuracy (Lele, 1992), its stencil forms a tridiagonal system which has to be solved with computational efficiency (see Martinez and Medeiros (2016) and Mathias and Medeiros (2018) for more details). To attenuate high-frequency noise, numerical low-pass filters are implemented in the domain and buffer zone (Gaitonde and Visbal, 1998). The stencil is adjusted few nodes from the wall for maintaining the dissipation in the leading order error, excepted at the wall, where it is not centered.

4. MESH INDEPENDENCE AND UNCERTAINTY QUANTIFICATION

The Fig. 3 presents the mesh spacing in the X and Y directions. From the Fig. 3a is possible to see that the maximum refinement is at the upstream wall of the roughness element. From the Fig. 3b is possible to see that the refinement near the wall is uniform up to 4 times the roughness element. The ratio between the minimum spacing in X and Y is 3.7.

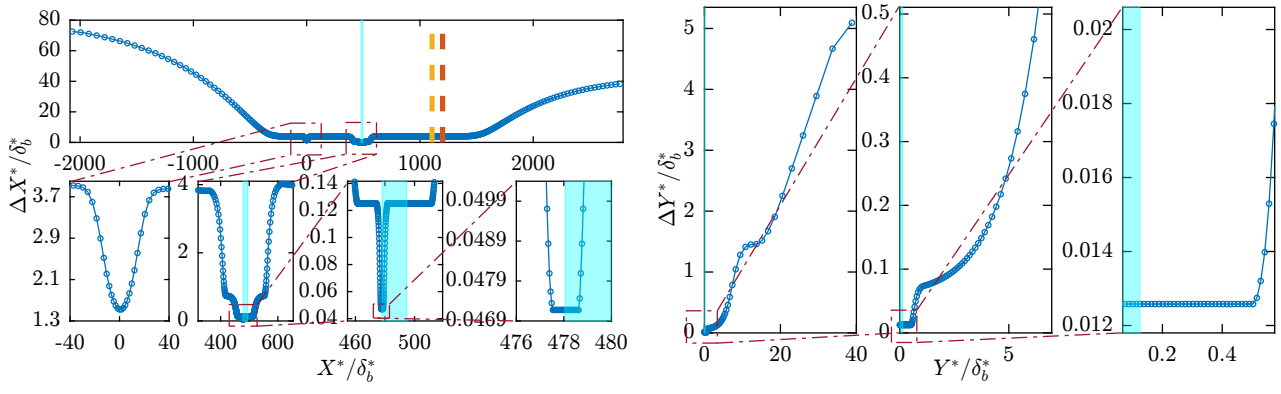

(a) X direction (b) Y direction

Figure 3. Mesh spacing in the a) X direction, and b) Y direction in different regions. The yellow dashed (- -) line represents the most downstream probe position from the experiment of Placidi *et al.* (2020). The red dashed (- -) line represents the buffer zone's edge. The cyan shaded rectangle represents the roughness' position.

The less is the Ma number, the fast is the acoustic wave in the simulation, which demands a smaller time step in order to maintain the numerical stability. The experiment of Placidi *et al.* (2020) were made at about Ma 0.054, so it was necessary to improve the Ma number to speed up the simulations. However, this change has to maintain the correlation with the experimental data within the overall uncertainty.

A parametric space was delineated to provide an uncertainty estimate. It concerns the mesh, domain, and Mach over the amplification of the TS wave at the plate with and without roughness. The uncertainty about the Mach number and the difference about the case with and without roughness are discussed herein, and the others are omitted.

The Fig. 4 shows the amplification of the TS wave inserted by a suction and blowing at the wall. The distance between the roughness and the source position were equal to three times the TS length. In this figure, the upper charts are the normalized amplification curves, and the down charts are the relative difference between the amplification curves. The relative difference are calculated by $100 * \| \left(\|TS\|_i - \|TS\|_{ref} \right) \| / \|TS\|_{ref}$, where $\|TS\|$ is the amplitude of the TS wave obtained via the Fast Fourier Transform (FFT). The left collum of Fig. 4 suggest that the Ma 0.10 carry out at least a 4% uncertainty, which was thought to be acceptable. Moreover, the right collum presents the relative difference between the amplification of the TS over the plate with and without roughness. These curves overlaps reasonable well and the difference at the end of the domain is 2%, which was thought to be in agreement with the results of Wörner *et al.* (2003).

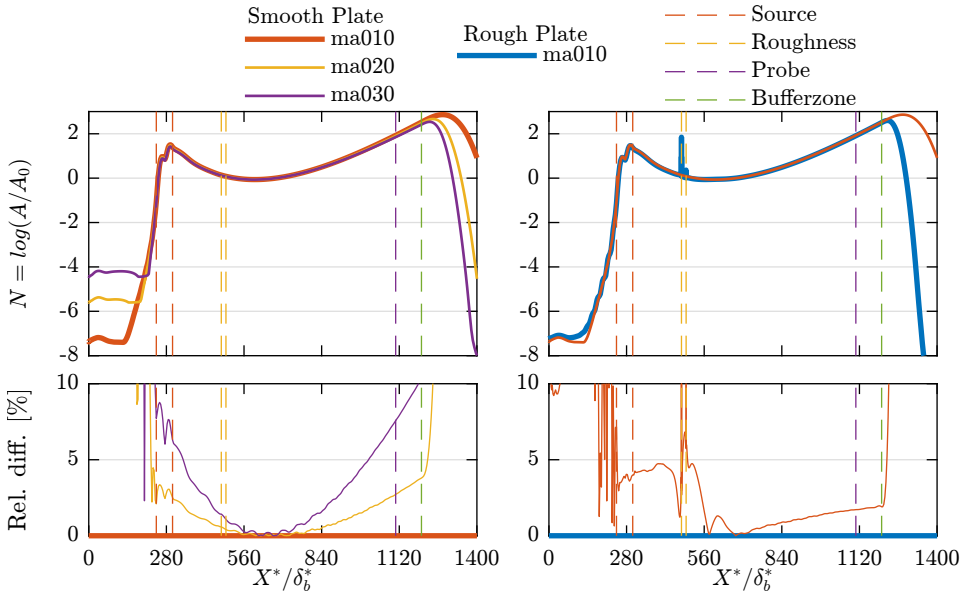

Figure 4. Amplification of a monochromic Tollmien-Schilchting wave inserted artificially at the wall. The left collum presents a comparison among the amplification over the smooth plate with Ma 0.10, 0.20, and 0.30. The right collum presents a comparison between the amplification of the T.S. over the smooth and the rough plate.

Figure 5 shows the mean flow distortion and the amplitude of the TS wave of the cases with and without roughness. It is possible to see that the increase in the mean flow distortion due to the roughness is negligible. Moreover, the mean flow distortion is of order $\mathcal{O}(10^{-5})$, which suggests that the non linear amplification effects are also negligible in this case.

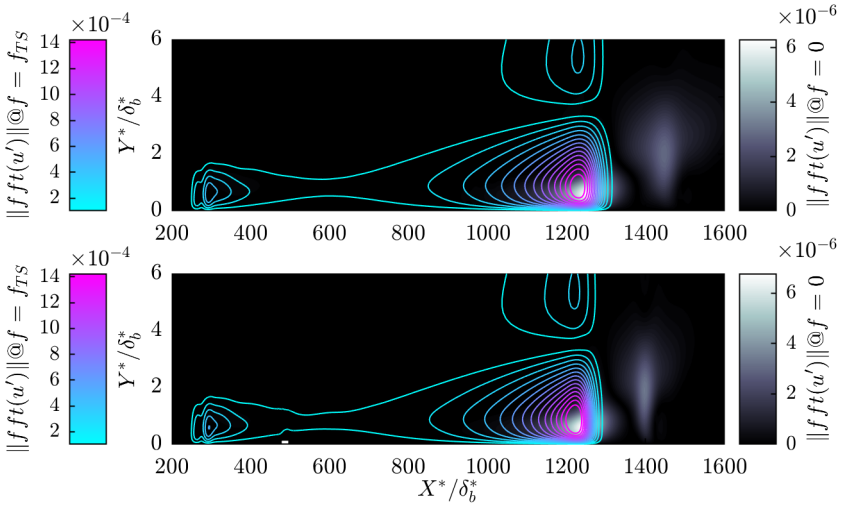

Figure 5. Mean flow distortion (dark background) and amplitude of the FFT at the TS frequency (light lines). The upper chart is the smooth plate, and the down chart is the roughness plate. The light lines are in the same levels in both charts.

Figure 6(a) shows the acoustic wave simulated and the acoustic wave calculated with the impedance constraint within

a free stream with uniform velocity. It is possible to see a remarkable agreement between these data. In the region of the Bufferzone, the acoustic disturbance in the simulation is damped.

Figure 6(b) presents the evolution in space and time of a 1 period of sinusoidal perturbation at the inflow. The data is in absolute value and the color is in logarithmic scale. It is possible to see that there is no reflection at the outflow, which is due to the mesh stretching and to the use of numerical damper.

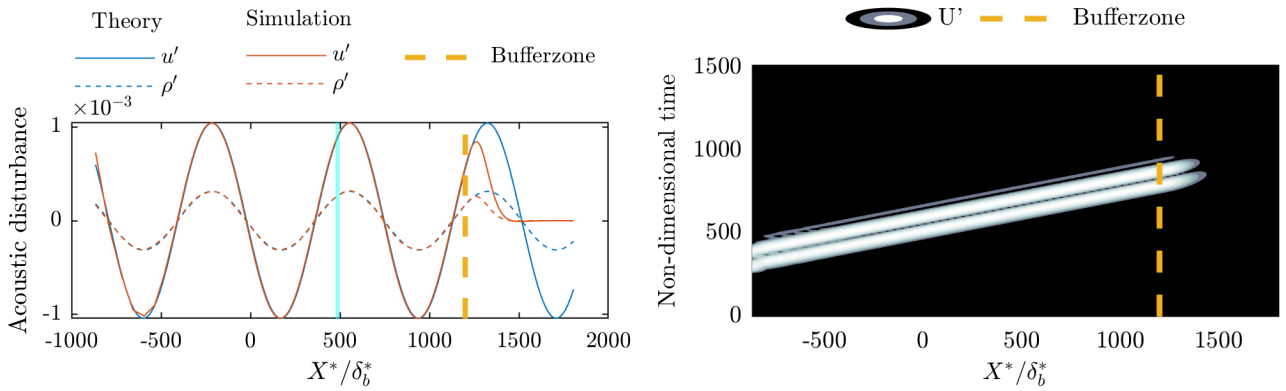

(a) Acoustic free stream disturbance

(b) 1 Period of acoustic excitation in free stream

Figure 6. The figure a) presents a comparison between the theoretical acoustic disturbance in the free stream flow and the simulated disturbance in the same physical parametric space of the flat plate's simulation. The cyan rectangle represents the virtual position of the roughness element. The figure b) presents the evolution in space and time of the absolute value of the excitation of 1 period of acoustic wave. The color scale is logaritimic.

5. FLOW VISUALIZATION

Figure 7(a) presents the baseflow over the plate with roughness. The upper chart shows the contour of the streamwise velocity in red. The black solid line is the position of δ_{99}. The Fig. 7(a) down charts are the stream lines near the upstream and downstream edges of the hump. It is possible to see a recirculation zone in the downstream edge.

Figure 7(b) presents the displacement thickness (δ^*) and momentum thickness (θ) near the hump, and compares with the respective thickness in the smooth plate. It is possible to see that the hump increase the δ^*. However, the θ increases and decreases with respect to the smooth plate.

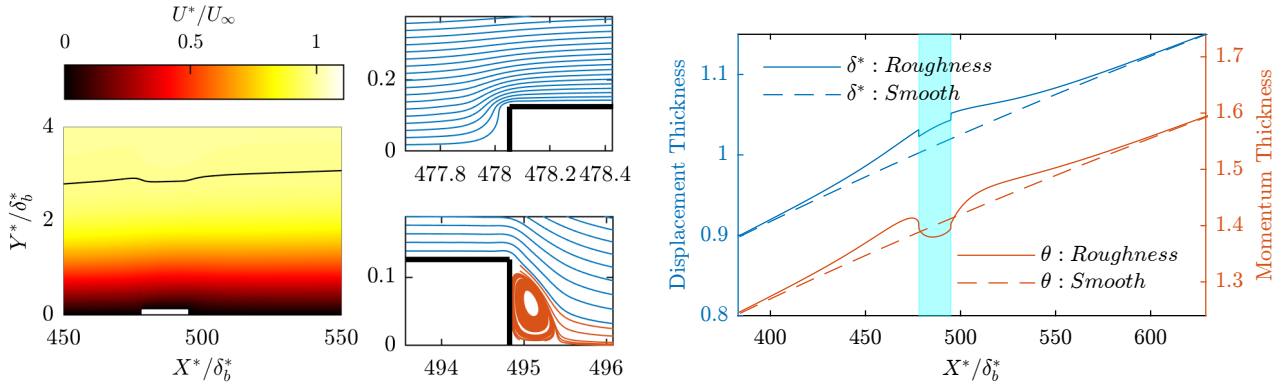

(a) Baseflow with roughness

(b) δ^* and θ over the smooth and rough plate

Figure 7. The figure (a) is the baseflow of the case with roughness. It presents the contour of the streamwise velocity in red. The continuos (–) black line is the δ_{99} of the baseflow. The cyan light lines are the streamlines. The figure b) presents the displacement thickness (δ^*) and momentum thickness (θ) over the rough and smooth plate. The cyan rectangle is at the roughness position.

Figure 8(a) presents the steady disturbance developed by the hump over the streamwise velocity. It is the difference between the baseflow with and without roughness. It is possible to see that this disturbance causes a decrease in velocity near the wall, and a increase of the velocity at about $Y = 3$.

Figure 8(b) presents the fluctuation (unsteady disturbance) over the (upper chart) smooth plate and (bottom chart) rough plate at the same given time. These fluctuation are obtained, for each case, by the difference of the case with acoustic incidence and the respective baseflow. It is possible to see that the acoustic disturbance, which is the black and

white vertical strips, are identical in both figures. It is also possible to see that the case with roughness (down chart) presented the TS wave, which is due to the receptivity mechanism. This TS is represented in the red contour lines.

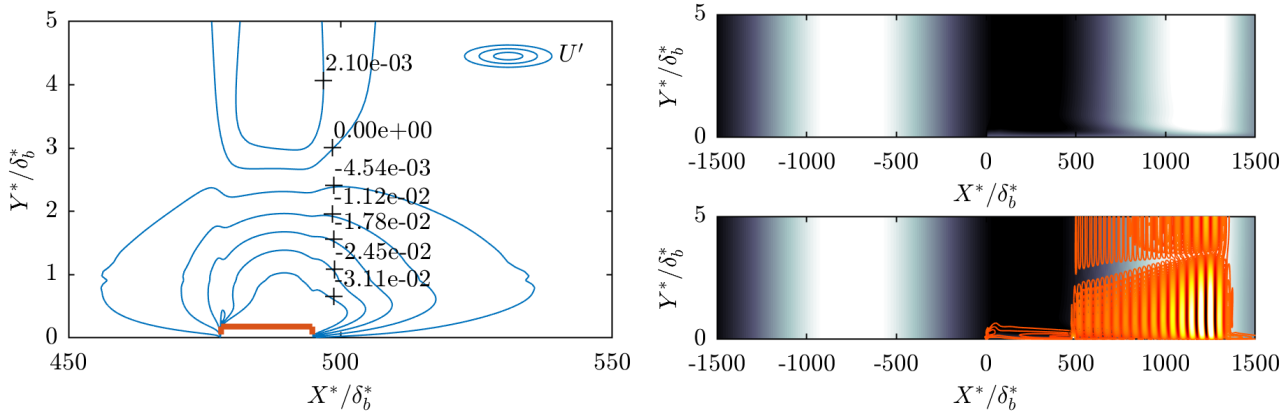

Figure 8. The left side a) is the contour lines of the baseflow's steady disturbance due to the roughness with respect to the velocity in the X-direction. It is calculated by the difference between the baseflow of the case with roughness and without roughness. The right side b) is the unsteady disturbance over the smooth (upper) and roughness (down) plate at a given time due to the acoustic incidence. The unsteady disturbance over the roughness plate have the TS wave inserted via receptivity

The TS wave generated via receptivity is filtered out of the complete flow solution by the subtraction of the fluctuation over the rough and smooth plate (i.e. , the difference between Fig. 8(b)(bottom) and 8(b)(top)). This subtraction is made with the flows ate the same simulation time. The result at a give time is present in Fig. 5(top). The Fig. 5(bottom) presents the mean flow distortion and the amplitude of the FFT at the TS frequency, It suggests that this TS wave is in the linear amplification regime.

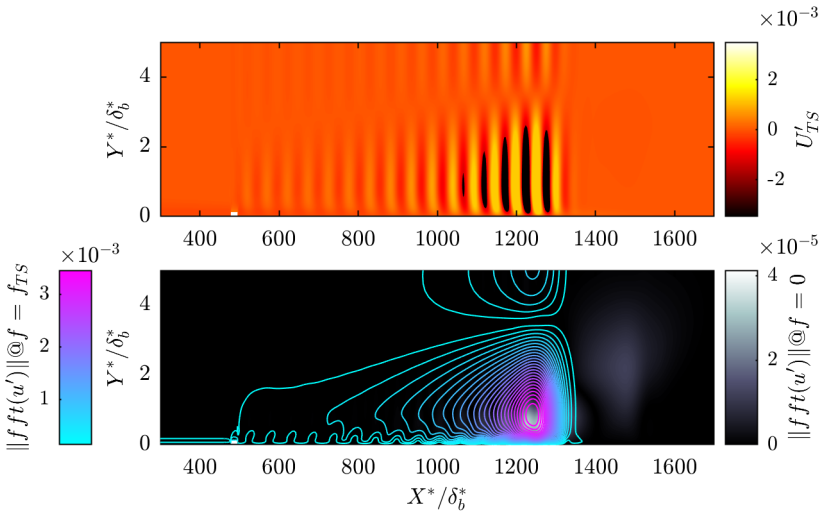

Figure 9. TS wave inserted via receptivity and the respective mean flow distortion and amplitude contour lines.

Figure 10 shows the maximum TS amplitude in each X position. The blue curve is the TS obtained via receptivity and the orange line is the TS obtained by suction and blowing at wall in the smooth plate. The orange line is normalized to match the amplitude of the TS generated via receptivity at the virtual position of the probe in the experiment of Placidi *et al.* (2020). This is done to encounter the initial amplitude of the TS as if it was in the smooth plate. This comparison provides a robust way to compare different experiments and simulations.

6. COMPARISON WITH EXPERIMENTAL DATA

Figure 11 compares the result of the TS obtained via receptivity in the present simulations at Ma 0.10 and in the experiment of Placidi *et al.* (2020). The simulated TS appears to have an identical auto function in the Y direction, and the Y position of the peak lobes are consistent with the experiment. However, the amplitude is different at about 40% with respect to the experiment.

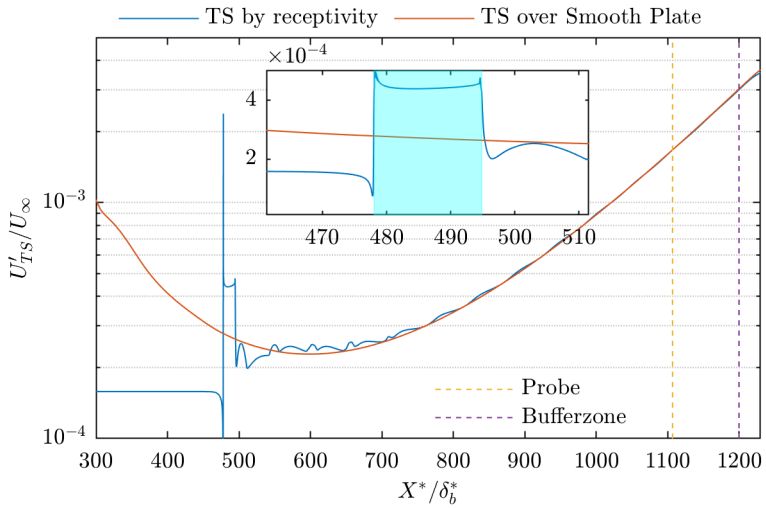

Figure 10. Comparison between the TS wave amplification of the receptivity case and of the smooth wall case.

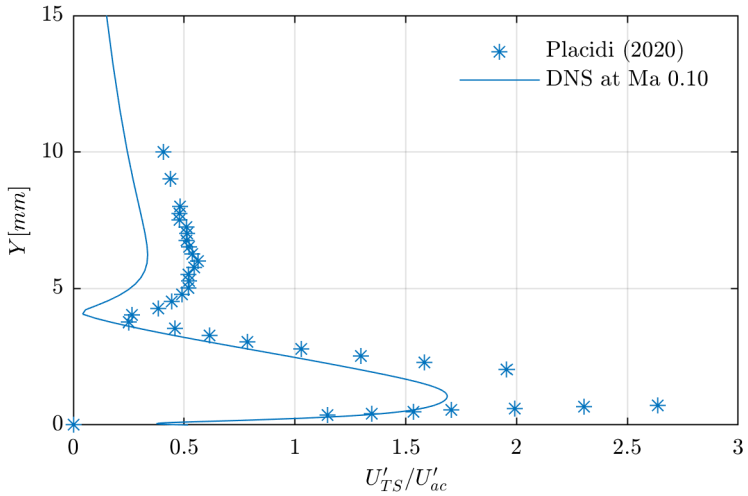

Figure 11. Amplitude of the TS wave at the probe position divided by the amplitude of the free stream acoustic wave. The solid (–) line is the data from the current simulation, and the star (*) points are the data present in Placidi *et al.* (2020).

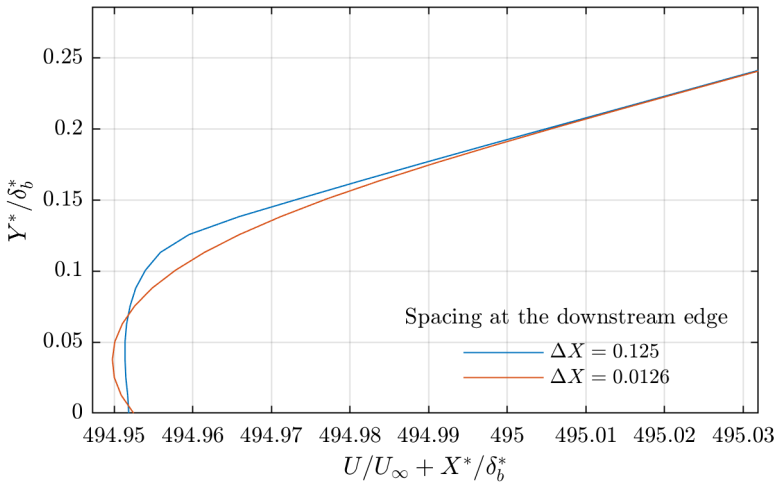

Figure 12. Velocity profile near the downstream edge of the roughness.

It is necessary to further investigate the reason of this discrepancy. The mesh and Ma independence in the amplification of the TS wave inserted artificially at wall presented reasonable well results (within 4% uncertainty). However, the mesh and Ma independence with respect to the amplitude at the roughness position (see Fig. 10) is yet to be done. Moreover, recent mesh analysis showed a discrepancy in the stream wise velocity near the backward facing wall of the hump, as it is

showed in Fig. 12. It suggests that the flow field is not independent of the mesh yet.

7. CONCLUSIONS AND NEXT STEPS

The results of these simulations may in the future complement those of earlier experimental and numerical studies, especially in the non-linear behavior. It is possible, for example, to obtain the mean flow distortion due to the TSW amplification at every position of the flow.

Although the results presented a discrepancy at about 40% with the experiment, it may be possible to obtain receptivity tendency curve and also the departure from linear regime threshold. To do so, it is necessary to run the simulations over a much larger parametric space.

For the next paper, it will be provided the mesh independence analysis in regards to the initial instability amplitude, according to the methodology present in Fig. 10.

8. ACKNOWLEDGEMENTS

The authors would like to thank the University of Liverpool for the access to the Barkla cluster, provided by Prof. Vassilios Theofilis. They also thank the Center for Mathematical Sciences Applied to Industry (CeMEAI), funded by São Paulo Research Foundation (FAPESP/Brazil) - grant 2013/07375-0, for access to the Euler cluster, led by Prof. José Alberto Cuminato. The authors acknowledge the National Laboratory for Scientific Computing (LNCC/MCTI, Brazil) for providing HPC resources of the SDumont supercomputer, which have contributed to the research results reported within this paper. URL: http://sdumont.lncc.br.

This study was financed in part by the Coordenação de Aperfeiçoamento de Pessoal de Nível Superior – Brasil (CAPES) – Finance Code 001, and FAPESP - project grant 2019/15336-7. Santos, P. H. R. is sponsored by CAPES grant no. 88882.379188/2019-01 and by FAPESP/Brazil grant no. 2020/04413-1. Himeno, F. H. T. is sponsored by FAPESP/Brazil grant no. 2018/02542-9. Mathias, M. S. is sponsored by FAPESP/Brazil grant no. 2018/04584-0. Medeiros, M. A. F. is sponsored by National Council for Scientific and Technological Development (CNPq/Brazil), grant no. 307956/2019-9 and the US Air Force Office of Scientific Research (AFOSR) for grant FA9550-18-1-0112, managed by Dr. Geoff Andersen from SOARD.

9. REFERENCES

Åkervik, E., Brandt, L., Henningson, D.S., Hœpffner, J., Marxen, O. and Schlatter, P., 2006. "Steady solutions of the Navier-Stokes equations by selective frequency damping". *Physics of Fluids*. ISSN 10706631. doi: 10.1063/1.2211705.

Crouch, J.D., 1992. "Localized receptivity of boundary layers". *Physics of Fluids A*, Vol. 4, No. 7, pp. 1408–1414. ISSN 08998213. doi:10.1063/1.858416.

De Tullio, N. and Ruban, A.I., 2015. "A numerical evaluation of the asymptotic theory of receptivity for subsonic compressible boundary layers". *Journal of Fluid Mechanics*, Vol. 771, pp. 520–546. ISSN 14697645. doi: 10.1017/jfm.2015.196.

Fransson, J.H.M., 2003. "Flow control of boundary layers and wakes". *Technical Reports from Royal Institute of Technologiy KTH Mechanics*, , No. December.

Gaitonde, D.V. and Visbal, M.R., 1998. "High-order schemes for Navier-Stokes equations: algorithm and implementation into FDL3DI". *Air Vehicles Directorate*.

Lele, S.K., 1992. "Compact finite difference schemes with spectral-like resolution". *Journal of Computational Physics*. ISSN 10902716. doi:10.1016/0021-9991(92)90324-R.

Martinez, G.A.G. and Medeiros, M.A.F., 2016. "Direct numerical simulation of a wavepacket in a boundary layer at Mach 0.9". In *46th AIAA Fluid Dynamics Conference*. American Institute of Aeronautics and Astronautics, Reston, Virginia. ISBN 978-1-62410-436-7. doi:10.2514/6.2016-3195. URL `http://arc.aiaa.org/doi/10.2514/6.2016-3195`.

Mathias, M.S. and Medeiros, M.A.F., 2018. "Direct Numerical Simulation of a Compressible Flow and Matrix-Free Analysis of its Instabilities over an Open Cavity". *Journal of Aerospace Technology and Management*, Vol. 10. ISSN 2175-9146. doi:10.5028/jatm.v10.949. URL `http://www.jatm.com.br/ojs/index.php/jatm/article/view/949`.

Morkovin, M.V., 1994. "Transition in open flow systems - a reassessment". *Bulletin of the American Physical Society*, Vol. 39, p. 1882.

Morkovin, M.V., 1969. "On the many faces of transition". In *Viscous drag reduction*, Springer, pp. 1–31.

Placidi, M., Gaster, M. and Atkin, C.J., 2020. "Acoustic excitation of Tollmien-Schlichting waves due to localised surface roughness". *Journal of Fluid Mechanics*, pp. 1–13. ISSN 14697645. doi:10.1017/jfm.2020.349.

Raposo, H., Mughal, S.M. and Ashworth, R., 2019. "An adjoint compressible linearised Navier-Stokes approach to model generation of Tollmien-Schlichting waves by sound". *Journal of Fluid Mechanics*, Vol. 877, pp. 105–129. ISSN 14697645. doi:10.1017/jfm.2019.601.

Ruban, A.I., 1984. "On the generation of Tollmien-Schlichting waves by sound". *Fluid Dynamics*, Vol. 19, No. 5, pp. 709–717. ISSN 1573-8507. doi:10.1007/BF01093536. URL https://doi.org/10.1007/BF01093536.

Saric, W.S., Reed, H.L. and Kerschen, E.J., 2002. "Boundary-Layer Receptivity to Freenstream Disturbances". *Annual Review of Fluid Mechanics*, Vol. 34, No. 1, pp. 291–319. ISSN 0066-4189. doi: 10.1146/annurev.fluid.34.082701.161921.

Wörner, A., Rist, U. and Wagner, S., 2003. "Humps/steps influence on stability characteristics of two-dimensional laminar boundary layer". *AIAA Journal*, Vol. 41, No. 2, pp. 192–197. ISSN 00011452. doi:10.2514/2.1960. URL http://arc.aiaa.org/doi/10.2514/2.1960.

10. RESPONSIBILITY NOTICE

The authors are solely responsible for the printed material included in this paper. The opinions, hypotheses and conclusions or recommendations expressed in this material are the responsibility of the author(s) and do not necessarily reflect the position of FAPESP.